Coherent splitting of single photons by an ideal beam splitter

J. D. Franson
Applied Physics Laboratory, The Johns Hopkins University, Laurel, Maryland 20723
(Received 29 January 1996)

It is shown that an ideal beam splitter has a small probability of splitting a single photon into a pair of secondary photons, conserving energy in the process. These nonlinear effects are a fundamental consequence of the quantization of the field and are analogous to other nonlinear effects in QED, such as the scattering of one photon by another. [S1050-2947(96)00706-8]

PACS number(s): 42.50.Ct, 42.50.Ar, 03.65.Bz, 12.20.Fv

It is commonly assumed that a single photon incident upon an ideal beam splitter must either be transmitted or reflected [1]. It is shown here, however, that an ideal beam splitter has a small probability of splitting a single photon into a pair of secondary photons, conserving energy in the process. These nonlinear effects are a fundamental consequence of the quantization of the electromagnetic field and are analogous to other nonlinear effects in QED, such as the scattering of one photon by another. They are due to the presence of the $\mathbf{A}^2$ term in the Hamiltonian and are not dependent on any nonlinear properties of the material comprising the beam splitter, unlike the situation in parametric down-conversion [2–4].

The origin of these effects can be most easily understood by considering the case of a metallic beam splitter, which will be analyzed in detail, after which some comments will be made with regard to the analogous situation in dielectrics. The valence electrons in a simple metal can be approximated as free particles provided that their momenta are not too large [5]. The low-frequency limit in which the photon momenta are much smaller than the Fermi momentum of the electrons (and the photon wavelengths are much larger than the thickness of the beam splitter) will therefore be considered. Scattering and other sources of dissipation will be ignored, in which case a metallic beam splitter can be modeled as a large number of free electrons confined to a potential well.

The beam splitter is assumed to have plane surfaces corresponding to $z=\pm a$ and to have infinite extent in the x and y directions as illustrated in Fig. 1. Periodic boundary conditions with period $2L$ will be applied in the x and y directions for the electrons and in the x, y, and z directions for the photons. For simplicity, the initial photons will be assumed to be incident on the beam splitter in the x-z plane at an angle of 45°, with their polarization $\hat{\epsilon}_0$ in the plane of incidence as shown in the figure.

The Hamiltonian in the Coulomb gauge is given by

$$H=\frac{1}{2m}\sum_i\left[\left(\frac{\hbar}{i}\boldsymbol{\nabla}_i-\frac{q}{c}\mathbf{A}\right)^2+q\boldsymbol{\Phi}\right]+\sum_{\mathbf{p}\hat{\epsilon}}\left(a^\dagger_{\mathbf{p}\epsilon}a_{\mathbf{p}\epsilon}+\frac{1}{2}\right)\hbar\omega_{\mathbf{p}} \tag{1}$$

as can be derived from the standard Lagrangian [6]. Here index i labels the electrons in the beam splitter, $a^\dagger_{\mathbf{p}\epsilon}$ creates photons of wave vector $\mathbf{p}$ and polarization $\hat{\epsilon}$, and $\mathbf{A}$ is the quantized vector potential operator. The scalar potential $\boldsymbol{\Phi}$ plays no role in the effects of interest here and can be ignored. Treating the interaction between the field and the electrons as a small perturbation gives the interaction Hamiltonian

$$H'=\sum_i\left(-\frac{q}{mc}\mathbf{A}\cdot\frac{\hbar}{i}\boldsymbol{\nabla}_i+\frac{q^2}{2mc^2}\mathbf{A}^2\right). \tag{2}$$

Lowest-order perturbation theory can be used if the beam splitter is sufficiently thin that most of the photons are simply transmitted. In that case the total rate Γ_2 at which the two-photon splitting occurs is given by the usual second-order perturbation theory

$$\Gamma_2=\frac{2\pi}{\hbar}\sum_{\mathbf{p}_1,\mathbf{p}_2}\sum_{\epsilon_1,\epsilon_2}\left|\sum_m\frac{\langle n|H'|m\rangle\langle m|H'|0\rangle}{E_0-E_m+i\eta\hbar}\right|^2\delta(E_n-E_0), \tag{3}$$

where $|m\rangle$ and $|n\rangle$ represent the intermediate and final states.

Diagram I of Fig. 2 corresponds to the absorption of an incident photon with wave vector $\mathbf{p}_0$ by the $\mathbf{j}\cdot\mathbf{A}$ term in H', after which a pair of photons with wave vectors $\mathbf{p}_1$ and $\mathbf{p}_2$ are emitted via the $\mathbf{A}^2$ term. The other five diagrams correspond to equivalent processes leading to the same final state. Since we want to consider the limit in which the properties of the medium do not play a significant role, it will be assumed that $\Delta E=E_0-E_m$ is dominated by the energies of the photons rather than that of the electrons; this is an excellent approximation for a metallic beam splitter, for example, where the recoil energy due to the absorption of a photon is relatively small. In that case

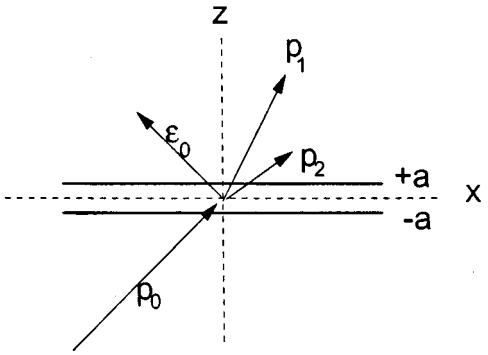

FIG. 1. Splitting of an incident photon by a thin metallic beam splitter.

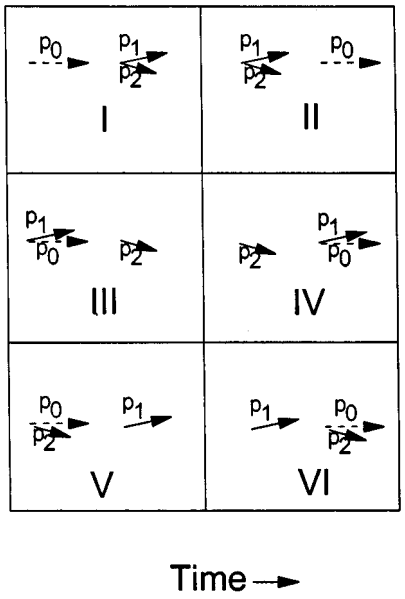

FIG. 2. Simplified diagrams for six processes leading to the same final state. The absorption of a photon is represented by a dashed line while emission is represented by a solid line. The $\mathbf{A}^2$ term is responsible for the two-photon events while the $\mathbf{j}\cdot\mathbf{A}$ term produces the single-photon events.

$$\Delta E_{\mathrm{I}} = \hbar\omega_0 = -\Delta E_{\mathrm{II}} \tag{4}$$

where the subscripts I and II refer to the first two diagrams of Fig. 2. The minus sign in Eq. (4) is essential to prevent cancellation between diagrams I and II, since it will be found that their matrix elements are equal in magnitude but opposite in sign. Similar comments apply to the other pairs of time-reversed diagrams in Fig. 2.

The boundary conditions at $z=\pm a$ quantize the z component of the electron momenta, so that the distribution of occupied electron states (in the limit of low temperature) consists of a series of parallel, circular disks inside the Fermi surface in momentum space as illustrated in Fig. 3. The infinite extent of the beam splitter in the x and y directions ensures that momentum is conserved in those directions,

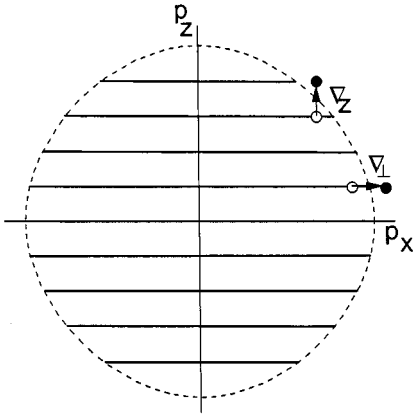

FIG. 3. Transitions from occupied to unoccupied energy levels in momentum space as produced by the two components of the gradient operator.

whereas it need not be conserved in the z direction. The initial state $|0\rangle$ can be written in the form [7]

$$|0\rangle = \prod_{k\leqslant k_F} \Psi_{k\pm}|\mathbf{p}_0, \hat{\boldsymbol{\epsilon}}_0\rangle, \tag{5}$$

where

$$\Psi_{k+} = c_n e^{ik_x x} e^{ik_y y} \cos\left[\frac{(n-1/2)\pi z}{a}\right],$$

$$\Psi_{k-} = c_n e^{ik_x x} e^{ik_y y} \sin\left[\frac{n\pi z}{a}\right] \tag{6}$$

represent the solutions with even and odd parity in z. Here n is a positive integer and c_n is a normalization constant. Antisymmetrization of the wave function has no effect on the results and can be ignored.

Because of the boundary conditions, it is necessary to separate the gradient operator into two components parallel and perpendicular to the z direction:

$$\boldsymbol{\nabla} = \boldsymbol{\nabla}_z + \boldsymbol{\nabla}_\perp . \tag{7}$$

First consider only the contribution of operator $\boldsymbol{\nabla}_z$ to diagram I, in which the incident photon is absorbed via the $\mathbf{j}\cdot\mathbf{A}$ term. The z dependence of $\boldsymbol{\nabla}_z$ can induce transitions from a $\Psi_\pm$ state to a higher-energy state of the opposite parity, as required for an allowed dipole transition. This can only occur, however, if the higher-energy state is unoccupied as illustrated by the upward arrow in Fig. 3.

The intermediate states in this case have the form

$$|m\rangle = \Psi_{k_2} \prod_{k\neq k_1} \Psi_k |0\rangle, \tag{8}$$

where $\mathbf{k}_1$ and $\mathbf{k}_2$ are the initial and intermediate momenta of an electron, respectively. The final state is then

$$|n\rangle = \prod_{k\leqslant k_F} \Psi_k |\mathbf{p}_1, \hat{\boldsymbol{\epsilon}}_1; \mathbf{p}_2, \hat{\boldsymbol{\epsilon}}_2\rangle, \tag{9}$$

where the polarizations $\hat{\boldsymbol{\epsilon}}_1$ and $\hat{\boldsymbol{\epsilon}}_2$ of photons 1 and 2 need not lie in the plane of incidence. The final electronic state must be the same as the initial state in order to maintain coherence; the probability of such events is greatly enhanced by the fact that all of the electrons in the beam splitter can then contribute coherently to the same final state.

It is then necessary to expand the momentum dependence of the $\mathbf{A}^2$ term to first order in evaluating the matrix elements from the intermediate to final state:

$$e^{-i(p_{1z}+p_{2z})z} = 1 - i(p_{1z}+p_{2z})z + \cdots . \tag{10}$$

The constant term in this expansion cannot contribute to the matrix element between two different states, so that the lowest-order contribution is proportional to $p_{fz}=p_{1z}+p_{2z}$. The product of the matrix elements can then be shown to be proportional to

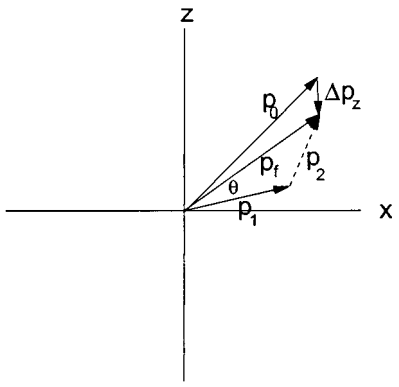

FIG. 4. Spherical coordinate system used to sum over the final photon states.

$$\langle n|H'|m\rangle\langle m|H'|n\rangle = (\hat{\boldsymbol{\epsilon}}_1\cdot\hat{\boldsymbol{\epsilon}}_2) f_L(k_{1x}+p_{0x}-k_{2x}) \times f_L(k_{1y}+p_{0y}-k_{2y}) f_L(k_{1x}+p_{fx}-k_{2x}) \times f_L(k_{1y}+p_{fy}-k_{2y}) \frac{n_1}{(\delta n+\frac{1}{2})^3} \times \epsilon_{0z}(p_{1z}+p_{2z}), \tag{11}$$

where f_L is a strongly peaked function (sinc function) in the limit of large L. Most of the contribution comes from $\delta n=0$, where $\delta n=n_2-n_1$ and n_1 and n_2 are the values of n for the initial and intermediate states. Larger values of δn will be neglected, which limits the initial states to those near the circumference of the disks in momentum space. The product of the matrix elements for diagram II can be shown to be the same as those of diagram I except for a minus sign, as mentioned above.

Now consider the contribution to diagram I from the operator $\boldsymbol{\nabla}_\perp$. This is limited to those states within $\mathbf{p}_0$ of an edge of a disk in momentum space, since the recoil from the absorption of a photon must carry the system from an occupied to an unoccupied state as illustrated by the horizontal arrow in Fig. 3. The matrix element from the initial state to the final state is now proportional to the initial electron momentum $\mathbf{k}_{1\perp}$ perpendicular to the z axis. This reverses sign for diagram II, since the recoil momentum will then be effective only on the other side of the disk where $\mathbf{k}_{1\perp}$ has the opposite sign. This sign reversal also cancels the change in sign of ΔE in Eq. (4), so that diagrams I and II once again interfere constructively. The product of the matrix elements is similar to that from the $\boldsymbol{\nabla}_z$ term, except that $\epsilon_{0z}(p_{1z}+p_{2z})$ is replaced by $\epsilon_{0x}p_{0x}$.

The total two-photon transition rate Γ_2 can be found by integrating Eq. (3) over all possible final states of the two secondary photons, which can be most easily accomplished using a spherical coordinate system centered about $\mathbf{p}_f=\mathbf{p}_1+\mathbf{p}_2$ as illustrated in Fig. 4. The independent variables are then the angles θ' and ϕ', the length of $\mathbf{p}_1$, and the displacement Δp_z of $\mathbf{p}_f$ from $\mathbf{p}_0$. Including the contributions from all six diagrams gives the total probability P_2 of a two-photon event:

$$P_2=\frac{2^{7/2}\alpha^3}{3^2\pi^{12}}(k_F\lambda_c)^4(k_Fa)^2c_{\mathrm{I}}. \tag{12}$$

Here c_{I} is a dimensionless integral defined by

$$c_{\mathrm{I}}=\sum_{\hat{\epsilon}_1,\hat{\epsilon}_2}\int_0^{\sqrt{2}}d\Delta p_z\int_0^{\pi}d\theta'\int_0^{2\pi}d\phi'\,\frac{p_1\sin\theta'}{(1-p_f\cos\theta')} \times\left[\frac{(\hat{\boldsymbol{\epsilon}}_1\cdot\hat{\boldsymbol{\epsilon}}_2)\hat{\boldsymbol{\epsilon}}_0\cdot\left(\mathbf{p}_{1z}+\mathbf{p}_{2z}+\frac{\pi^2}{8}\mathbf{p}_{0\perp}\right)}{p_0} + \frac{(\hat{\boldsymbol{\epsilon}}_1\cdot\hat{\boldsymbol{\epsilon}}_0)\hat{\boldsymbol{\epsilon}}_2\cdot\left(\mathbf{p}_{0z}-\mathbf{p}_{1z}+\frac{\pi^2}{8}\mathbf{p}_{2\perp}\right)}{p_2} + \frac{(\hat{\boldsymbol{\epsilon}}_2\cdot\hat{\boldsymbol{\epsilon}}_0)\hat{\boldsymbol{\epsilon}}_1\cdot\left(\mathbf{p}_{0z}-\mathbf{p}_{2z}+\frac{\pi^2}{8}\mathbf{p}_{1\perp}\right)}{p_1}\right]^2, \tag{13}$$

while k_F is the electron wave vector at the Fermi surface, λ_c is the Compton wavelength of the electron, and α is the fine structure constant. All of the photon wave vectors in Eq. (13) are normalized to the magnitude of $\mathbf{p}_0$.

The integral in Eq. (13) can be evaluated numerically using the Monte Carlo technique, which gives an approximate value of $c_{\mathrm{I}}=23.4$. This is also a convenient way to include experimental factors such as the limited solid angle subtended by a pair of detectors. A silver beam splitter ($k_F=1.19\times10^{10}$/m) with a thickness of 10 nm gives $P_2=3\times10^{-14}$.

The rate Γ_1 at which photons polarized perpendicular to the plane of incidence are simply reflected by the beam splitter in the usual way can also be calculated using the same assumptions. In that case the $\mathbf{A}^2$ term annihilates an incident photon and immediately emits a photon of the same frequency into another direction. The results of that calculation are in reasonable agreement with the experimentally observed reflectivity of thin metallic films. The ratio R of the number of photons that are split to the number that are simply reflected is given by

$$R=\frac{\Gamma_2}{\Gamma_1}=\frac{2^{7/2}\alpha}{\pi^6}\left(\frac{\lambda_c}{\lambda_0}\right)^2c_{\mathrm{I}}, \tag{14}$$

where λ_0 is the wavelength of the incident photons. It can be seen that R is independent of the properties of the beam splitter, including its thickness, for the conditions considered here. $R=0.96\times10^{-13}$ at a typical laser wavelength of 351 nm.

Although the probability of splitting a photon is relatively small, coincidence measurements at low incident intensities

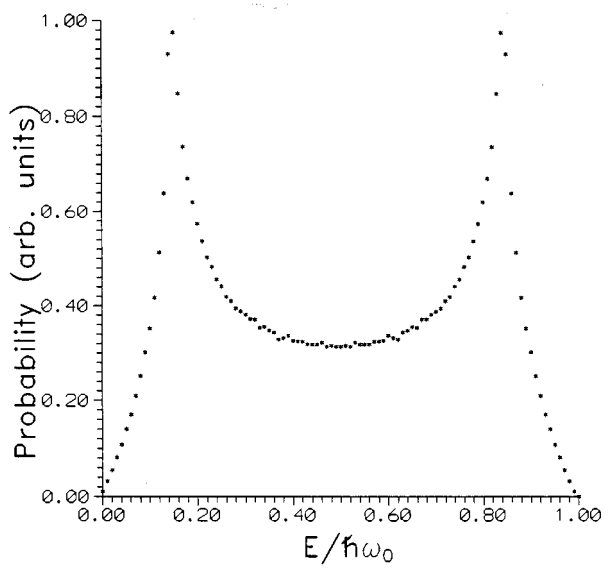

FIG. 5. Spectrum of the secondary photons in arbitrary units. $E/\hbar\omega_0$ is the energy of the photons normalized to that of the incident photon.

can minimize the accidental rate from fluorescence and other effects. Counting rates on the order of one event per hour should be achievable in experiments of this kind. This estimate is based on Monte Carlo calculations corresponding to an incident laser intensity of 2 mW with solid angles, detection efficiencies, and other experimental conditions typical of those commonly used in two-photon correlation experiments. The dark counting rates (noise) of commercially available detectors are sufficiently low that there should be no difficulty in observing such an effect using coincidence time windows on the order of 100 ps, which are readily achievable.

The predicted spectrum of the secondary photons is shown in Fig. 5 and is also independent of the properties of the beam splitter. Two peaks corresponding to stationary (saddle) points occur at photon energies of $E=\hbar\omega_0/[4(1\pm 1/\sqrt{2})]$.

Although momentum is not conserved in the z direction, energy conservation still restricts the final momentum to the specular direction for the case of single photons reflected in the usual way (Γ_1). That does not occur, however, in the two-photon case (Γ_2), where the additional degrees of freedom in the final momenta allow the secondary photons to be emitted into all directions. Thus there is no phase-matching condition analogous to that of parametric down-conversion.

The free-electron model used here is not suitable for dielectric materials, where the $(\mathbf{j}\cdot\mathbf{A})^2$ term can no longer be neglected and tends to cancel the $\mathbf{A}^2$ term; this reflects the fact that the electrons in a dielectric are bound and have a more limited response to an external electric field. In the limit of bound electrons, one is led instead to the conventional theory [2] of parametric down-conversion in nonlinear crystals, which is based on third-order perturbation theory involving three allowed (dipole) transitions between bound states. Since there are then three atomic states involved, at least one of the transitions would have to be a ''forbidden'' transition between two states of the same parity if all of the states had well-defined parity; this can be avoided only if parity is destroyed by an asymmetry of the crystal lattice. In addition, the factor of $1/\Delta E$ can be enhanced if one or more of the virtual states is near a resonance. Thus the usual nonlinear properties of such a material are dependent upon its asymmetries and energy levels, unlike the situation considered here. It should be noted that second and third harmonic generation at the surfaces of nonlinear materials have been extensively investigated [8].

Although the effects described here and parametric down-conversion correspond to the opposite limits of free vice bound electrons, there is an obvious similarity between the two and they both produce correlated pairs of photons. The main point of this paper is that nonlinear effects of this kind are unavoidable when the field is quantized and that they need not rely on any inherently nonlinear properties of the material, as illustrated by Eq. (14).

The nonclassical nature of the photon splitting is evident from the fact that the corresponding classical model of free electrons in a metal would only lead to Ohm's law [9], which is strictly linear and cannot produce any subharmonics. The essential difference between classical theories and the quantum theory can be better understood by considering a classical theory involving a nonlinear (anharmonic) potential $U(x)$ of the form

$$U(x)=c_2x^2+c_3x^3+\cdots , \tag{15}$$

where c_2 and c_3 are arbitrary coefficients. The origin of such a nonlinearity is not relevant here, but could involve the Coulomb interaction between the electrons associated with cooperative phenomena such as plasmons, for example. Regardless of their origin, the nonlinear terms become negligibly small in the limit of small displacements about the equilibrium point, which will be the case if the external driving field is sufficiently weak. In contrast, Eq. (14) shows that the relative magnitude of the nonlinear quantum effects depends only on the wavelength of the incident light and not its intensity. It is interesting to note that a similar dependence on the incident wavelength instead of the classically expected intensity also occurs in the photoelectric effect, which led to Einstein's work on the nature of the photon. The fact that nonlinear effects must vanish in the limit of low intensities in the classical theory but not in the quantum theory is a remarkable difference between the two theories, as has been discussed previously [10].

It is also interesting to note that no $\mathbf{A}^2$ term explicitly appears in the Hamiltonian in a relativistic treatment of QED. The $\mathbf{A}^2$ term can be shown to arise in the nonrelativistic limit of QED as a result of second-order processes corresponding to the creation and annihilation of virtual electron-positron pairs. That is also the case for other nonlinear effects in QED, such as the scattering of one photon by another [11], and all of these nonlinear effects are a fundamental consequence of the quantization of the field.

The author is grateful to Jonathan Dowling, R. Vyas, and S. Singh for their comments. This work was supported by the Office of Naval Research.

[1] For example, see R. A. Campos, B. E. A. Saleh, and M. C. Teich, Phys. Rev. A **40**, 1371 (1989).

[2] Ya. B. Zel'dovich and D. N. Klyshko, Zh. Eksp. Teor. Fiz. Pis'ma Red. **9**, 69 (1969) [JETP Lett. **9**, 40 (1969)]; Sov. J. Quantum Electron. **10(9)**, 1112 (1980); D. N. Klyshko, *Photons and Nonlinear Optics* (Gordon and Breach, New York, 1988).

[3] D. C. Burnham and D. L. Weinberg, Phys. Rev. Lett. **25**, 84 (1970).

[4] J. D. Franson, Phys. Rev. Lett. **62**, 2205 (1989); **67**, 290 (1991).

[5] C. Kittel, *Introduction to Solid State Physics* (Wiley, New York, 1968).

[6] C. Cohen-Tannoudji, J. Dupont-Roc, and G. Grynberg, *Photons and Atoms-Introduction to Quantum Electrodynamics* (Wiley, New York, 1989).

[7] If the incident photon is in the form of a broad wave packet so that the interaction is limited to a finite time interval Δt, then the eigenstates and physical observables of the system are apparent both before and after the interaction.

[8] C. C. Wang and E. L. Baardsen, Phys. Rev. **185**, 1079 (1969); J. E. Sipe, D. J. Moss, and H. M. van Driel, Phys. Rev. B **35**, 1129 (1987).

[9] One might ask whether or not Ohm's law would apply to a classical model of the situation considered here, since the effects of dissipation and scattering have been ignored. But the inertia of an electron limits its response to a high-frequency external electric field, giving rise to a complex conductivity that remains finite even in the limit of no dissipation or scattering. In fact, the conductivity of metallic films at sufficiently short wavelengths is limited by just these kinds of effects and Ohm's law still applies with a complex conductivity. [For example, see M. Born and E. Wolf, *Principles of Optics* (Pergamon, New York, 1980).]

[10] J. D. Franson, Phys. Rev. A **45**, 8074 (1992).

[11] M. Delbruck, Z. Phys. **84**, 144 (1933); R. Karplus and M. Neuman, Phys. Rev. **83**, 776 (1951).